Rock abundance on the lunar mare on surfaces of different age: Implications for regolith evolution and thickness

Sashank Vanga[1]

Caleb I. Fassett[2]

Michael Zanetti[2]

Cole Nypaver[3]

Bradley J. Thomson[3]

Masatoshi Hirabayashi[4]

[1] Department of Space Science, The University of Alabama in Huntsville

[2] Heliophysics and Planetary Science Branch, NASA Marshall Space Flight Center

[3] Department of Earth and Planetary Sciences, University of Tennessee, Knoxville

[4] Department of Aerospace Engineering, Auburn University

Corresponding author: Caleb Fassett (caleb.i.fassett@nasa.gov)

Key Points:

- Crater frequency and age of mare units are inversely correlated with rock abundance, consistent with regolith thickening over time.
- On old surfaces with thick regolith, the median rock abundance is non-zero, consistent with re-excavation of rocks from within the regolith.
- The half-life of meter-scale surface rocks as derived in the work presented here is 80±20 Myr.

Abstract

The growth of lunar regolith over time affects surface rock abundance, because larger, less frequent impacts are needed to penetrate thicker regolith developed on older surfaces and excavate rocks. On younger surfaces with thinner regolith, smaller, more frequent impacts are sufficient to excavate rocks. We quantify the correlation between observed rock abundances and age on the lunar surface by comparing Diviner rock abundance data to the surface ages of inter-crater parts on the maria. Our observations show the expected negative correlation between age and rock abundance. The commonality of non-zero rock abundance values on ancient surfaces, combined with a simple Monte Carlo model of the rock excavation process, suggest that rocks re-excavated from the regolith volume contribute to the presently observed rock population on the lunar surface. The half-life of meter-scale surface rocks most consistent with our observations is 80±20 Myr.

Plain Language Summary

The lunar surface is covered by regolith, which includes particles ranging in size from dust to boulders. Past work has suggested that regolith is meters to tens-of-meters thick, with average thickness increasing with terrain age. At least in the maria, beneath the regolith is fragmental bedrock. When impacts large enough to penetrate the regolith occur, boulders from this underlying bedrock are excavated onto the surface. Excavating boulders is expected to be more difficult where the regolith is thicker, because thicker regolith limits the ability of craters to eject material from the underlying fragmental bedrock. This implies larger and rarer impacts are needed to excavate rocks on older terrain. We tested this idea by comparing the rock abundance data from the Diviner Lunar Radiometer Experiment on the Lunar Reconnaissance Orbiter spacecraft with previously obtained crater statistics for part of the maria, excluding the area within and immediately adjacent to D≥1 km craters. We show that older maria have, on average, lower fractional rock abundances, consistent with a thicker regolith on older surfaces influencing rock excavation. Rocks excavated from within the regolith are necessary to be consistent with the continued presence of non-zero rock abundance on old terrains.

1. Introduction

The surface of the Moon is covered by regolith, a layer of poorly sorted particles ranging in size from dust to boulders, the median particle size of which is very fine sand (Carrier et al., 1991). Because of its ubiquity, the regolith is primarily what we observe on the Moon with remote sensing instruments and is the material we interact with when exploring the lunar surface. Many of the important geological, geochemical, mineralogical, and geotechnical characteristics that define lunar regolith were established by the Apollo missions and its precursors (e.g., McKay et al., 1991). Modern remote sensing methods allow us to extrapolate regolith characteristics from landing sites to places that have not yet been explored in situ.

The existing paradigm for regolith growth and evolution is that it is dominated by impact cratering and gardening (e.g., Shoemaker et al., 1967; McKay et al., 1991; Costello et al., 2018). Because of the similarity between impacts and explosions, this can be thought of as an explosive demolition process. Using the Neukum production function (NPF) for the Moon combined with scaling calculations to determine the size of impactors (Ivanov, 2001), the kinetic energy delivered by impacts over the last 3 Ga that formed 10 m $\leq$ D $\leq$ 500 m craters is ~3–6×10^{15} J/km^2, approximately equivalent to a megaton of TNT/km^2, with ~10^4 unique events/km^2. This demolition process is why there is almost no bedrock exposed on the Moon's upper surface, the median grain size of the surface has been reduced to very fine sand, and regolith thickens with time.

Several of the instruments on the Lunar Reconnaissance Orbiter (LRO) have provided new data relevant to rock populations and regolith evolution, particularly the Lunar Reconnaissance Orbiter Camera (LROC) (Robinson et al., 2010), the Diviner Lunar Radiometer Experiment (Paige et al., 2010; Hayne et al., 2017), and Miniature Radio Frequency (Mini-RF) radar (e.g., Nozette et al., 2010; Raney et al., 2011; Cahill et al., 2014). Many analyses of these data have focused on the rock abundance in craters' ejecta (Ghent et al., 2014; Fassett et al., 2018; Mazrouei et al., 2019; Nypaver et al., 2021), rather than in the inter-crater regions of the maria. Additionally, the abundance of meter-scale rocks has also been manually assessed with LROC in a few selected areas of particular interest, such as landing sites (Li et al., 2017; Wu et al., 2018; Watkins et al., 2019), as well as on a more global basis with machine learning (Bickel et al., 2020). By looking at craters of different ages, LROC imaging allowed an estimate of the

half-life of rocks (≥2 m) as 40–80 Myr (e.g., Basilevsky et al., 2013). The half-life here is defined as the period where 50% of simultaneously exposed rocks in a population would be destroyed; or, equivalently, the period that any given rock has a 50% chance of survival after exposure. This short lifetime implies that rocks on the lunar surface are very susceptible to destruction by impacts (Hörz et al., 2020) and by other processes such as thermal fatigue (e.g., Molaro et al., 2017). However, craters and landforms older than 300 Myr can maintain an excess of nearby meter-scale rocks for much longer than the lifetime of individual rocks (Ghent et al., 2014; Bickel et al., 2020; Nypaver et al., 2021). Two factors may contribute to this persistent excess of rocks. First, regolith mobility in areas of substantial topographic relief can allow exhumation of rocks from the subsurface. Second, around the D=18-90 km craters considered by Ghent et al. (2014), the initial excavated rock population likely includes rocks much bigger (10m and above) than those looked at by Basilevsky et al. (2013) that may take additional time to be destroyed.

Past work has suggested that bedrock is converted to regolith on the Moon at a rate of order ~1–2m/Gyr (Langevin and Arnold, 1975; Hörz et al., 1991; Xie et al., 2021) so that regolith thickness correlates reasonably well with unit surface age (e.g., Shkuratov and Bondarenko, 2001; Fa et al., 2014). However, there are three subtleties regarding the thickening of regolith with time, evident from Monte Carlo modeling (e.g., Oberbeck et al., 1973; Quaide and Oberbeck, 1975) and theory (Hirabayashi et al., 2018). First, the actual rate of regolith growth is faster when and where the regolith is thin; as a result, regolith growth slows with time (Oberbeck and Quaide, 1968). This is because smaller craters that form more frequently can only create new regolith when the depth to underlying fragmental bedrock is sufficiently thin (e.g., Fig. 1).

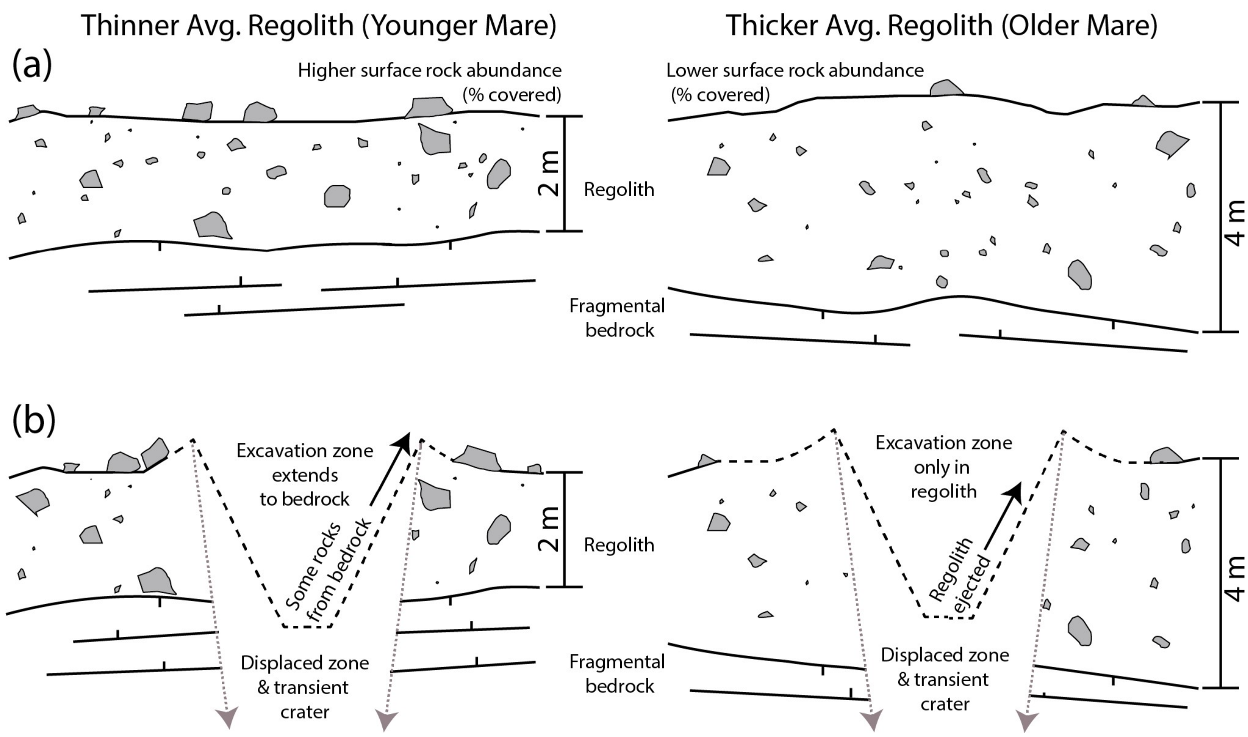

Figure 1. The hypothesis for this paper is that (a) younger areas will have thinner average regolith and more rocks at the surface. As illustrated in (b), a small crater (~10-20 m in diameter, vertical exaggeration ~10×) can excavate through a thinner regolith layer but not a thicker regolith area. On average, this makes ejected blocks from underlying bedrock more common on younger, thinner regolith areas.

Second, even in a local area of a given age, i.e., on an individual mare flow unit, there is expected to be an appreciable range in regolith thickness (e.g., Oberbeck and Quaide, 1968; Wilcox et al., 2005; Bart et al., 2011; Hirabayashi et al., 2018; Yue et al., 2019), so describing only the central tendency (median or average) of regolith thickness neglects a substantial amount of variability. The reason for this intra-unit variability is that regolith thickness is highly sensitive to the size and distance of the nearby largest craters ejecting regolith or brecciating material on their interior (e.g., Hirabayashi et al., 2018). As a result of this variability, the distribution of regolith thickness around the median or expected value for a given surface is not symmetric. A small fraction of area on a local terrain can have much thicker regolith than normal (perhaps several multiples of the median), whereas the thinnest part of the regolith is closer to the median (see, e.g., Hirabayashi et al. 2018; their Fig. 10).

Third, we might expect the rate of regolith thickening was much higher early in the history of the Moon, because the impact rate was higher. For example, with the NPF flux, an equivalent number of craters are expected to be produced in the last 1 Ga as in 100 Ma between

3.37 and 3.47 Ga. Since the bulk of the maria were emplaced >3.3 Ga (e.g., Hiesinger et al., 2011), the regolith on the maria may predominantly be expected to have mostly formed in early time periods and been augmented by slower growth rates in the last billion years. While this general trend may remain correct, regolith thickness evolution may be more complicated if there was a shift in the shape of the impactor population's size-frequency distribution along with the increased flux, as recently suggested by Xie et al. (2021).

The hypothesis of this study is that the abundance of rocks in low-relief areas of the maria should be sensitive to regolith thickness, and thus surface age (see Fig. 1; also note that an inverse correlation between the abundance of rocks and regolith thickness has been suggested at the Surveyor landing sites (e.g., Shoemaker and Morris, 1970)). The basic reason for this expected sensitivity is that the rock population of the lunar surface is controlled by how many rock-excavating craters can form over the comparatively short lifetime of surface rocks (i.e., Fig. 1). Where regolith is thinner, smaller, more frequent impacts can excavate rocks; where regolith is thicker, larger, less frequently occurring impacts are needed. The goal of this study is to evaluate the correlation between rock abundance and surface age and use these observations to refine the model of regolith evolution.

We address this hypothesis using observations from Diviner rock abundance data (Bandfield et al., 2011) combined with mapped crater density information from Fassett and Thomson (2014). In the discussion, we also describe a simple Monte Carlo model of lunar surface rock abundance that we have used to better understand the observations.

2. Data and Methods

For this project, the main dataset is lunar rock abundance derived from Diviner observations (Bandfield et al., 2011; 2017). This Diviner rock abundance map was derived by fitting the measured nighttime thermal radiance with a two-component model assuming the observed scene is a mixture of fine-grained material and rock. The resulting map pixels represent the areal fraction of the surface covered by rock fragments roughly ≥1 m (cf. Bandfield et al., 2017). Diviner-derived rock abundances have been validated with what is observed in LROC data (Bandfield et al., 2011), and LROC-derived rock abundance appears to agree reasonably with what is estimated at landing sites (e.g., Watkins et al., 2019).

To estimate unit surface ages, we rely on measurements of surface crater densities from Fassett and Thomson (2014). They mapped 13,657 craters in the D=800 m to 5 km size range on a portion of the mare (see their Fig. 1), selected to exclude areas near very large, post-mare craters (D≥20 km) as well as to manually exclude areas with chains of obvious secondaries. Fassett and Thomson (2014) generated a crater density map of these craters in 50 km-radius moving neighborhoods at 5 km spatial resolution (hereafter referred to as neighborhood crater frequency) (see their Fig. 5a). An advantage of this type of moving neighborhood method (e.g., Ostrach and Robinson, 2014) is that it is strictly based on mapped superposed craters, so it is not reliant on other geologic inputs to derive crater statistical information. For analysis, these crater frequencies are converted to ages using the NPF chronology model (Ivanov, 2001) from the formation rate of D=800 m-5 km craters (see supplement text S1). The systematic uncertainty in our ages thus inherits uncertainties underlying the NPF chronology (e.g., complexities related to landing site geology, secondary contamination, etc).

Diviner rock abundance pixels were extracted and assigned their corresponding neighborhood crater frequency. To focus our dataset primarily on inter-crater regions, we also excluded the rock abundance/crater frequency pairs for the portions of the maria within one crater diameter of the rim of D≥1 km craters based on the crater catalog of Robbins (2019). This does not exclude the contribution of these D≥1 km craters to the neighborhood crater frequencies or ages, but does exclude them from the analysis of how the rock abundance evolves. The resulting total study are was 1.54×10^6 km^2, approximately 25% of the maria, incorporating 33.2×10^6 rock abundance pixels. The data from thesse regions were sorted by increasing neighborhood crater frequency and grouped into 100 bins using python library pandas' qcut function. This function bins the Diviner data into constant-size groups (3.3×10^5 per bin) based on frequency. The reason this statistical approach is necessary is that rock abundances are expected to be highly stochastic: even for units of the same age and regolith thickness, the rock abundance should be expected to vary significantly based on the size and recency of rock-excavating craters. Binning together a large number of pixels with consistent crater frequency (or, equivalently, a large amount of area of equivalent age), this effect can be minimized, and overall trends revealed. The distribution of rock abundance values at a given locale was then assessed by extracting the 5th-, 50th- (median), mean, and 95th-percentile of the rock abundance values in each age bin-defined measurement area. The median frequencies for these groups are equivalent

in the NPF chronology to expected crater population accumulated on surfaces over ~0.5 Ga to 3.7 Ga.

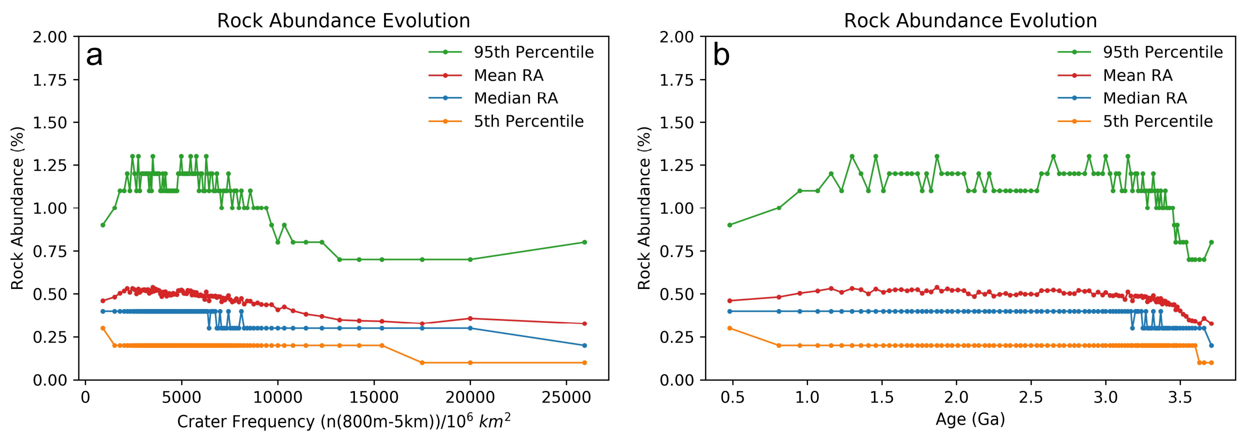

Figure 2. (a) Results for Diviner rock abundance (y-axis) vs. neighborhood crater frequency (x-axis) on surfaces in 50-km radius moving neighborhoods. (b) Results for Diviner rock abundance (y-axis) vs Neukum model age in billions of years (x-axis). The mean rock abundance slowly declines with increasing crater frequency / age. Because craters accumulated faster before 3 Ga, the decline in rock abundance is most prominent on the oldest surfaces (see Figure S1 in the supporting information for a detail of (b) from 3.0 to 3.75 Ga).

3. Results

The observed median, mean, 5th-percentile, and 95th-percentile rock abundances on the maria are shown as a function of neighborhood crater frequency in Figure 2a, and as equivalent model ages in Figure 2b. The model ages in Figure 2b come from the same data as 2a, with the x-axis rescaled to convert the neighborhood crater frequencies to ages using the NPF chronology.

Overall, the median and 5th-percentile of rock abundances show a nearly monotonic decline in rock abundance as a function of neighborhood crater frequency in Fig. 2a. The observed decline is nonlinear because it convolves several underlying complex processes (i.e., the cratering and regolith growth rates). The oscillatory behavior of the median for n(0.8–5 km) ~6000–8000 craters/10^6 km^2 (ages ~3.1–3.4 Ga) is due to the fact that the Planetary Data System-released Diviner fractional rock abundances values were stored with precision of 0.001 (0.1%), so all the percentile values match this fixed level of precision as well. The mean rock abundances

given in Fig. 2 are less affected by this fixed precision but are more sensitive to the rockiest fraction on surfaces of a given age than the median.

As a function of age (Fig. 2b), the median rock abundance is observed to be essentially constant for surfaces <3.1 Ga at 0.4%, decreases for surfaces >3.1 Ga to 0.3%, and to 0.2% at 3.7 Ga. The 5th-percentile (least rocky part of surfaces of a given age) declines from 0.3% in the youngest bin (~0.44 Ga) to 0.2% from ~0.77–3.6 Ga, to 0.1% at 3.7 Ga. Many of the least rocky areas of the Moon still have non-zero rock abundance (Bandfield et al., 2011), even in the highlands, and our 5th-percentile values here are not exceptional in never reaching 0.0%. The 95th-percentile (rockiest part of surfaces of a given age) initially increases in rock abundance, from 0.9% in the youngest bin, to 1.2% from ~1.2 Ga to ~3.3 Ga, then declines back to 0.7–0.8% >~3.5 Ga. The decreasing rock abundance trend in Fig. 2 for all series are statistically significant using the Mann-Kendall test (Hussain and Mahmud, 2019), as is the decline in rock abundance with frequency and age in the raw dataset as a whole (see supporting Text S2). However, this relationship is noisy and only holds when analyzed statistically or aggregated over large surface areas. For a given location, the rock abundance is not a useful predictor of age since it is contingent on the specific cratering history at that location.

The first five bins with the lowest nearby crater density (i.e., youngest surroundings, <1 Ga-equivalent model age) in Fig. 2 are anomalous in two respects. First, the 95th-percentile and mean rock abundance increase with age (or neighborhood crater frequency) in those bins, unlike the behavior of the rest of the data. Second, the equivalent model ages for these surfaces are lower than expected, given either (a) the age of mare basalts in existing sample collections or (b) the inferred age of units when measured at larger scales than 50-km. The most likely source for this anomaly is small number statistics, i.e., a 50 km radius was not enough to adequately sample the density of craters on sparsely cratered and relatively young terrains. In other words, these observed low neighborhood frequencies may be the stochastically less cratered fraction of older geologic units, rather than broad surfaces that are truly geologically young. It is thus somewhat uncertain how robust the behavior we see in these lowest neighborhood frequency/youngest age bins is.

Excluding the five bins with the lowest neighborhood crater frequency, the 95th-percentile rock abundance (the rockiest part of the surface for a given age/frequenc) declines

more quickly than the median rock abundance, which declines more than the 5th-percentile. In other words, we see the rockiest fraction of old terrain getting less rocky faster than its typical rock abundance.

4. Discussion, Comparison to Earlier Work, and Summary

4.1 Observed evolution of rock abundance with time

The fact that rock abundance statistics are all strongly correlated with neighborhood crater frequency (and thus age), and decline nearly smoothly for surfaces >1 Ga, supports the interpretation that regolith thickness is an important factor in controlling the observed rockiness of its surface. Additionally, the trends in rock abundance we observe with time, especially the much faster decline in rock abundance on surfaces older than ~3.1 Ga, are consistent with the exponentially higher impact flux early in lunar history that helped especially thicken the regolith on older terrains.

4.2 Monte Carlo modeling of mare rock abundance

To better understand how cratering and regolith thickness control the rock abundance, we have written a simple Monte Carlo model of the rock excavation process to compare with our observations (see also supporting Text S3 and repository code). For the growth of regolith, our model follows Hirabayashi et al. (2018), which reproduces observed constraints on thickening of the regolith on the mare well. Craters are generated at a rate defined by the NPF chronology model and production function to cover the size range of D =10 m to 800 m craters; additionally, craters are generated in the D=5–10 m range using an impactor production function based on Grün et al. (1985). To a first approximation, craters with diameter greater than ten times the local thickness of the regolith are assumed to excavate rocks from the fractured bedrock at depth (e.g., Croft, 1980; Melosh, 1989).

The main free parameters of the model are (a) the proximal rock abundance from new bedrock-excavating craters (rocks coming from bedrock), RA_{exc}; (b) the proximal rock abundance produced by new craters that do not reach bedrock (rocks coming from the existing regolith volume), RA_{reg}; and (c) the surface half-life of rocks, $\tau_{½}$. Values for these parameters most consistent with observations were determined using a grid search. The mean, 5th, 50th, and 95th-percentiles of the model results and data were compared from 0.5 to 3.7 Ga. We also

artificially assign a non-zero regolith thickness at the start of the simulation, which improves the fit on young surfaces. This is needed because we do not simulate D < 5 m craters that contribute to the rapid growth of the initial regolith thickness. Variations in this artificial initial thickness parameter from 0 to 2-m do not affect the best-fit physical parameters, but do improve the quality of the best-fit.

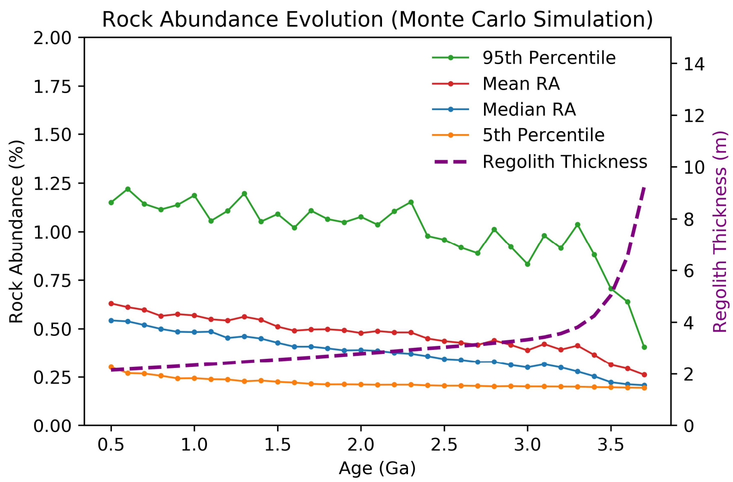

Figure 3. Best-fit Monte Carlo model of rock abundance evolution with time. The thicker regolith on earlier surfaces is why rock abundance is lower on surfaces >3 Ga.

The best-fit model results are given in Fig. 3. This model has rock abundance from bedrock-excavating craters RA_{exc}=0.08±0.02, rock abundance from the regolith of RA_{reg} =0.004±0.001, and half-life of surface rocks $\tau_{½}$=80±20 Myr; error ranges were the fits with median symmetric accuracy of <25% (Morley et al., 2018). In a broad sense, this simplified Monte Carlo model does a reasonable job of reproducing the rock abundance evolution. With these best-fit parameters, rock exposure is most influenced by craters that form frequently but still reach beneath the regolith in the D=10–25 m size range; for the rockiest pixels (95th-percentile), larger crater sizes of D=40–100 m are more important.

The model observations provide strong constraints on the allowable parameters. For example, it is impossible to get a 5th-percentile rock abundance at 1 Ga that matches observations unless the half-life of surface rocks is small, $\tau_{½}$<150 Ma. Likewise, on old surfaces (>3.5 Ga), the 5th-percentile and median rock abundance are impossible to reproduce unless the fraction of rocks RA_{reg} coming from within the regolith is non-zero: otherwise the regolith is sufficiently thick on surfaces this old to prevent craters from replenishing surface rocks. This is

highly consistent with the interpretation of Elder et al. (2019), who note that a sharp, single transition between regolith and underlying coherent rock cannot explain the observed rock abundance trends.

We note there is a tradeoff between the rock abundance from bedrock-excavating craters, RA_{exc}, and the rock half-life $\tau_{½}$ parameters: lower values of RA_{exc} need a larger $\tau_{½}$ to fit observations, and larger values of RA_{exc} need a smaller $\tau_{½}$ to fit observations. There are independent observational constraints that suggest RA_{exc} ~0.04–0.10 (e.g., South Ray + North Ray; Ghent et al., 2014), although these are derived for larger craters than are important in this model. Nonetheless, our results are consistent with these independent constraints. For the half-life of surface rocks, our estimates are in close agreement with the values determined by Basilevsky et al. (2013) of 40–80 Myr, though at the upper end of their range. Diviner data are sensitive to slightly smaller rocks (~1 m) than the rocks visible in LRO (≥2 m). It is plausible that there is a slight increase in the half-life of rocks as rock size decreases, although this is not required by our results.

The qualitative ways that the model disagrees with the observations are twofold. First, we do not observe the uptick in the 95th-percentile or mean rock abundance at young ages. As noted earlier, this observation is based on only five bins, and thus may not be that robust. Second, the model shows a steadier decline in rock abundance over time than the data, for any set of parameters. This disagreement between the model and observations may be a consequence of the limited precision of the rock abundance data, the limited fidelity of the neighborhood crater frequency for discerning the local age, the simplifying assumptions of the model, or some combination of these factors.

This Monte Carlo model is meant to be exploratory and is not intended to capture the full details of cratering, regolith gardening, or rock excavation. A few simplifications of this model are worth noting. Like Hirabayashi et al. (2018), the model neglects the lateral mobility of regolith (and rocks) driven by topography or slopes. The model also does not include non-local sources of rocks, such as from distal ejecta. Although rocks from distal ejecta likely occur on the Moon, the average contribution of distal rocks is likely minor, since geochemical evidence supports the interpretation that regolith is mostly locally derived (e.g., Papike et al., 1982). Our measurements are also averaged over wide areas of maria of the same surface age. This is only

globally representative if rock excavation and destruction occurs at the same rate across the surface. There is some evidence that some particular mare regions are unusually rocky for their age (e.g., Humorum) (Hayne et al., 2017; Haber et al., 2018; Nypaver et al., 2022) that are worth examining more closely in future work.

4.3. Comparison with Earlier Work

A past preliminary analysis of how rock abundance values compare to age was presented by Haber et al. (2018). They used the mapped ages of units from crater counts by Hiesinger et al. (2010), and also found a negative correlation between median rock abundance and age (see also Figure S2). They also stated that the 95th-percentile RA value behaved similarly to the median. Overall, their findings agree with our analysis, although our two analytical approaches differ in some significant ways. The crater mapping underlying the Hiesinger et al. (2010) model ages used by Haber et al. are better informed by geological assessment of unit boundaries than the data we use from Fassett and Thomson (2014), but the Hiesinger et al. count areas for sampling were relatively small, so ages on broader mare units are extrapolated. The neighborhood crater frequency data used here are not extrapolated – there is a frequency and thus model age calculated at every pixel – and thus cover more of the maria, but it does not separate individual units as cleanly. The effects of this are mitigated by the way we bin large areas. Our strategy of excluding regions near $D \geq 1$ km craters from the rock abundance analysis (though not from contributing to neighborhood crater frequencies) also helps to focus the analysis on the intercrater parts of the mare, where the background regolith development process is most important compared to earlier work. Regardless, the agreement of the present results with earlier work helps support the idea that an observable change in rock abundance occurs with unit age.

Xie et al. (2021) have used proxies for regolith thickness at several sites on the Moon (anchored by the Apollo and Luna sites) to argue that the regolith thickened less quickly before 3.5 Ga than expected, which they suggest may imply a shift in the impactor population prior to 3.5 Ga. Our data and modeling do not reveal this slower-than-expected growth in regolith prior to 3.5 Ga. Instead, we would argue that the rockiness we observe on mare units 3.5–3.7 Ga is reconcilable with expected regolith growth with a consistent impactor population and the expected higher impact flux. However, both Xie et al. and our measurements are indirectly sensitive to regolith thickness. More in-situ measurements of regolith thickness, particularly

capable of accounting for its variability even on a single geologic unit, would be very valuable to test these ideas. This could presumably be accomplished by a long-range lunar rover if outfitted with appropriate geophysical instrumentation.

4.4. Summary and conclusions

Comparing Diviner rock abundance values to surface ages, we demonstrate that the rock abundance on the maria decreases with neighborhood crater frequency and age in a significant way. The rock abundance on maria units declines more quickly on surfaces older than 3.3 Ga, consistent with thicker regolith due to the higher impact flux early in the Imbrian period.

We find a geologically short half-life of meter-scale surface rocks of 80±20 Ma is most consistent with our observations. This estimate also agrees with boulder lifetimes derived from LROC observations of rocks in crater ejecta by Basilevsky et al. (2013). Because of this short lifetime, our modeling suggests the rock abundance would be reduced below what is observed if rocks were sourced only from bedrock. This supports a recent finding of Elder et al. (2019) that re-excavation of rocks from within the regolith are important to the observed surface rock abundances. Overall, these results provide valuable information about how rock populations on the surface of the Moon evolve that can help understand landing sites that may be visited in the next decade.

Acknowledgments

SV and MZ acknowledge funding from the NASA Lunar Data Analysis Program. We thank two anonymous reviewers for constructive and clarifying suggestions that helped improve the manuscript.

Data and Model Availability

Data and code to help reproduce the results of this paper have been released to Zenodo. The code repository is available at doi:[10.5281/zenodo.6012585](https://doi.org/10.5281/zenodo.6012585) (also available at github, https://github.com/cfassett/MareRockAbundances); the raw extracted data is in at archive with doi: [10.5281/zenodo.6011671](https://doi.org/10.5281/zenodo.6011671).

References

Bandfield, J. L., Ghent, R. R., Vasavada, A. R., Paige, D. A., Lawrence, S. J., & Robinson, M. S. (2011). Lunar surface rock abundance and regolith fines temperatures derived from LRO Diviner radiometer data. *JGR-Planets*, *116*, E00H02. https://doi.org/10.1029/2011JE003866

Bandfield, J. L., Cahill, J. T., Carter, L. M., Neish, C. D., Patterson, G. W., Williams, J. P., & Paige, D. A. (2017). Distal ejecta from lunar impacts: Extensive regions of rocky deposits. Icarus, 283, 282–299. https://doi.org/10.1016/j.icarus.2016.05.013

Bart, G.D., Nickerson, R.D., Lawder, M.T., Melosh, H.J. (2011). Global survey of lunar regolith depths from LROC images, *Icarus*, *215*, 485–490. https://doi.org/10.1016/j.icarus.2011.07.017

Basilevsky, A., Head, J., & Horz, F. (2013). Survival times of meter-sized boulders on the surface of the Moon. *Planetary and Space Science*, *89*, 118– 126. https://doi.org/10.1016/j.pss.2013.07.011

Bickel, V.T., Aaron, J., Manconi, A., Loew, S., Mall, U. (2020). Impacts drive lunar rockfalls over billions of years. *Nature Communications*, *11*, 2862. https://doi.org/10.1038/s41467-020-16653-3

Cahill, J. T., Thomson, B., Patterson, G. W., Bussey, D. B. J., Neish, C. D., Lopez, N. R., Turner, F. S., Aldridge, T., McAdam, M., Meyer, H., Raney, R., Carter, L., Spudis, P., Hiesinger, H., & Pasckert, J. (2014). The miniature radio frequency instrument's (Mini-RF) global observations of Earth's Moon. *Icarus*, *243*, 173– 190. https://doi.org/10.1016/j.icarus.2014.07.018

Carrier, W. D., Olhoeft, G. R., & Mendell, W. (1991). Physical properties of the lunar surface. In *Lunar sourcebook: : A user's guide to the Moon*, 475– 594. New York: Cambridge University Press. https://www.lpi.usra.edu/publications/books/lunar_sourcebook/pdf/Chapter09.pdf

Costello, E.S., Ghent, R.R., & Lucey, P.G. (2018). The mixing of lunar regolith: Vital updates to a canonical model. *Icarus*, *314*, 327-344. https://doi.org/10.1016/j.icarus.2018.05.023

Croft, S.K. (1980), Cratering flow fields: Implications for the excavation and transient expansion stages of crater formation, *Proc. LPSC 11th,* 2347-2378.

Elder, C. M., Douglass, B., Ghent, R. R., Hayne, P. O., Williams, J.-P., Bandfield, J. L., & Costello, E. (2019). The subsurface coherent rock content of the Moon as revealed by cold-spot craters. *JGR-Planets*, *124*, 3373–3384. https://doi.org/10.1029/2019JE006128

Fa, W., Liu, T., Zhu, M.-H., and Haruyama, J. (2014), Regolith thickness over Sinus Iridum: Results from morphology and size-frequency distribution of small impact craters, *J. Geophys. Res. Planets, 119,* 1914– 1935, doi:10.1002/2013JE004604.

Fassett, C. I., & Thomson, B. J. (2014). Crater degradation on the lunar maria: Topographic diffusion and the rate of erosion on the Moon. *JGR-Planets*, *119*, 2255– 2271. https://doi.org/10.1002/2014JE004698

Fassett, C. I., King, I. R., Nypaver, C. A., & Thomson, B. J. (2018). Temporal evolution of S-band circular polarization ratios of kilometer-scale craters on the lunar maria. *Journal of Geophysical Research: Planets*, 123, 3133–3143. https://doi.org/10.1029/2018JE005741

Ghent, R. R., Hayne, P. O., Bandfield, J. L., Campbell, B. A., Allen, C. C., Carter, L. M., & Paige, D. A. (2014). Constraints on the recent rate of lunar ejecta breakdown and implications for crater ages. *Geology, 42*(12), 1059– 1062. https://doi.org/10.1130/G35926.1

Grün, E., Zook, H.A., Fechtig, H., Giese, R.H. (1985), Collisional balance of the meteoritic complex, Icarus, 62, 244-272, doi: 10.1016/0019-1035(85)90121-6

Haber, J.T., Hayne, P.O., Elder, C.M. (2018). Rock abundance and surface ages in the lunar maria. 49th Lunar and Planetary Science Conference, abs. no 2463. https://www.hou.usra.edu/meetings/lpsc2018/pdf/2463.pdf

Hayne, P. O. et al. (2017). Global regolith thermophysical properties of the Moon from the Diviner Lunar Radiometer Experiment. *JGR-Planets*, *122*, 2371– 2400. https://doi.org/10.1002/2017JE005387

Hiesinger, H., Head, J. W., Wolf, U., Jaumann, R., & Neukum, G. (2010). Ages and stratigraphy of lunar mare basalts in Mare Frigoris and other nearside maria based on crater size-frequency distribution measurements. *JGR-Planets*, 115, E03003, doi:10.1029/2009JE003380

Hiesinger, H., Head, J., Wolf, U., Jaumann, R., & Neukum, G. (2011). Ages and stratigraphy of lunar mare basalts: A synthesis. *GSA Special Papers*, *477*, 1– 51. https://doi.org/10.1130/2011.2477(01)

Hirabayashi, M., Howl, B., Fassett, C., Soderblom, J., Minton, D., & Melosh, H. (2018). The role of breccia lenses in regolith generation from the formation of small, simple craters: Application to the Apollo 15 landing site. *JGR-Planets*, 123, 527– 543.

Hörz, F., Grieve, R., Heiken, G., Spudis, P., & Binder, A. (1991). Lunar surface processes. In *Lunar sourcebook: A user's guide to the Moon*, 61– 120. New York: Cambridge University Press. https://www.lpi.usra.edu/publications/books/lunar_sourcebook/pdf/Chapter04.pdf

Hörz, F., Basilevsky, A.T., Head, J.W., & Cintala, M.J., (2020). Erosion of lunar surface rocks by impact processes: A synthesis. *Planetary and Space Science*, *194*, 105105. https://doi.org/10.1016/j.pss.2020.105105

Hussain, Md. M. and Mahmud, I. (2019). pyMannKendall: a python package for non parametric Mann Kendall family of trend tests. *Journal of Open Source Software*, *4*(39), 1556, https://doi.org/10.21105/joss.01556

Ivanov, B. A. (2001), Mars/Moon cratering rate ratio estimates, *Space Sci. Rev., 96,* 87–104, doi:10.1023/A:1011941121102.

Langevin, Y., & Arnold, J. R. (1977). The evolution of the lunar regolith, *Annual Review of Earth and Planetary Sciences*, 5(1), 449– 489. doi: 10.1146/annurev.ea.05.050177.002313.

Li, B., Ling, Z., Zhang, J., & Chen, J. (2017). Rock size-frequency distributions analysis at lunar landing sites based on remote sensing and in-situ imagery. *Planetary and Space Science, 146*, 30–39. https://doi.org/10.1016/j.pss.2017.08.008

Mazrouei, S. Ghent, R.R., Bottle, W.F., Parker, A.H., Gernon, T.M. (2019). Earth and Moon impact flux increased at the end of the Paleozoic, *Science*, *363*, 253–257, https://doi.org/10.1126/science.aar4058.

McKay, D.S., Heiken, G., Basu, A., Blanford, G., Simon, S., Reedy, R., French, B.M., & Papike, J. (1991). The lunar regolith. In *Lunar sourcebook: A user's guide to the Moon*, 285-356. New York: Cambridge University Press. https://www.lpi.usra.edu/publications/books/lunar_sourcebook/pdf/Chapter07.pdf

Melosh, H.J. (1989). *Impact Cratering: A Geologic Process.* Oxford: Oxford Univ. Press*,* 245pp.

Molaro, J. L., Byrne, S., & Le, J.-L. (2017). Thermally induced stresses in boulders on airless body surfaces, and implications for rock breakdown. *Icarus*, *294*, 247– 261. https://doi.org/10.1016/j.icarus.2017.03.008

Morley, S. K., Brito, T. V., & Welling, D. T. (2018). Measures of model performance based on the log accuracy ratio. Space Weather, 16, 69–88. https://doi.org/10.1002/2017SW001669

Nozette, S., et al. (2010). The lunar reconnaissance orbiter miniature radio frequency (Mini-RF) technology demonstration. *Space Sci. Rev., 150*, 285– 302, doi:10.1007/s11214-009-9607-5.

Nypaver, C.A., Thomson, B.J., Fassett, C.I., Rivera-Valentín, E.G., & Patterson, G.W. (2021). Prolonged rock exhumation at the rims of kilometer-scale lunar craters. *JGR-Planets*, *126*, e2021JE006897, doi:10.1029/2021JE006897.

Nypaver, C. A., Thomson, B. J., & Fassett, C. I. (2022). Investigating tectonically-induced mass wasting as a cause for enhanced boulder populations on the lunar maria. *Lunar Planet. Sci. Conf.*, *53,* abs. no. 2145.

Oberbeck, V., Quaide, W.L. (1968). Genetic implications of lunar regolith thickness variations, *Icarus, 9*, 446–465.

Oberbeck, V., Quaide, W., Mahan, M., & Paulson, J. (1973). Monte Carlo calculations of lunar regolith thickness distributions. *Icarus*, *19*(1), 87– 107. https://doi.org/10.1016/0019-1035(73)90141-3

Ostrach, L.R., Robinson, M.S. (2014). Areal Crater Density Analysis of Volcanic Smooth Plains: Mare Imbrium, A Revised Approach, *Lunar and Planetary Sci. Conf., 45,* 1266.

Paige, D. A., et al. (2010). The Lunar Reconnaissance Orbiter Diviner Lunar Radiometer Experiment. *Space Sci. Rev., 150*(1–4), 125– 160, doi: 10.1007/s11214-009-9529-2.

Papike, J.J., Simon, S.B., Laul, J.C. (1982). The Lunar Regolith' Chemistry, Mineralogy, and Petrology. *Rev. of Geophysics and Space Physics, 20*, 761-826, https://dx.doi.org/10.1029/RG020i004p00761.

Quaide, W. & Oberbeck, V. (1975). Development of the mare regolith: Some model considerations. *The Moon*, *13*, 27–55, doi: 10.1007/BF00567506.

Raney, R. K., et al. (2011), The lunar Mini-RF Radars: Hybrid polarimetric architecture and initial results, *Proc. IEEE*, *99*(5), 808–823, doi:10.1109/JPROC.2010.2084970.

Robbins, S. J. (2019). A new global database of lunar impact craters >1–2 km: 1. Crater locations and sizes, comparisons with published databases, and global analysis. *JGR-Planets*, *124*, 871– 892. https://doi.org/10.1029/2018JE005592

Robinson, M. S., et al. (2010). Lunar Reconnaissance Orbiter Camera (LROC) Instrument Overview, *Space Sci. Rev., 150*, 81– 124, doi:10.1007/s11214-010-9634-2.

Shkuratov, Y.G., Bondarenko, N.V. (2001). Regolith Layer Thickness Mapping of the Moon by Radar and Optical Data, *Icarus*, *149*, 329-338. https://doi.org/10.1006/icar.2000.6545

Shoemaker E.M., Batson R.M., Holt H.E., Morris E.C., Rennilson J.J., & Whitaker E.A. (1967). Surveyor V: Television pictures. *Science*, *158* 642-652. 10.1126/science.158.3801.642

Shoemaker, E. M., and Morris, E. C. (1970), Physical Characteristics of the Lunar Regolith Determined From Surveyor Television Observations, Radio Sci., 5(2), 129– 155, doi:10.1029/RS005i002p00129.

Watkins, R. N., Jolliff, B. L., Mistick, K., Fogerty, C., Lawrence, S. J., Singer, K. N., & Ghent, R. R. (2019). Boulder distributions around young, small lunar impact craters and implications for regolith production rates and landing site safety *JGR-Planets*, *124*, 2754–2771. https://doi.org/10.1029/2019JE005963

Wilcox, B.B., Robinson, M.S., Thomas, P.C., Hawke, B.R. (2005). Constraints on the depth and variability of the lunar regolith, *Meteoritics and Planetary Science, 40,* 695-710. https://doi.org/10.1111/j.1945-5100.2005.tb00974.x

Wu, B., Huang, J., Li, Y., Wang, Y., & Peng, J. (2018). Rock abundance and crater density in the candidate Chang'E-5 landing region on the Moon. *Journal of Geophysical Research: Planets*, *123*, 3256–3272. https://doi.org/10.1029/2018JE005820

Xie, M., Xiao, Z., Xu, L., Fa, W., & Xu, A. (2021). Change in the Earth–Moon impactor population at about 3.5 billion years ago. *Nature Astronomy*, *5*, 128–133. https://doi.org/10.1038/s41550-020-01241-8

Yue, Z., Di, K., Liu, Z., Michael, G., Jia, M., Xin, X., Liu, B., Peng, M., & Liu, J. (2019), Lunar regolith thickness deduced from concentric craters in the CE-5 landing area, *Icarus*, *329*, 46-54.

Geophysical Research Letters

Supporting Information for

Rock abundance on the lunar mare on surfaces of different age: Implications for regolith evolution and thickness

Sashank Vanga[1]
Caleb I. Fassett[2]
Michael Zanetti[2]
Cole Nypaver[3]
Bradley J. Thomson[3]
Masatoshi Hirabayashi[4]

[1]Department of Space Science, The University of Alabama in Huntsville
[2]Heliophysics and Planetary Science Branch, NASA Marshall Space Flight Center
[3]Department of Earth and Planetary Sciences, University of Tennessee, Knoxville
[4]Department of Aerospace Engineering, Auburn University

Contents of this file

Introduction

The supporting information includes additional model description and two additional figures showing derived rock abundance observations.

Text S1. Conversion of n(0.8-5km) Crater Frequencies to Model Age

The crater measured in Fassett and Thomson (2015) were all between 800m and 5km. Conversion of these to an equivalent model age based on the Neukum chronology can be accomplished as follows, where capital N(X) represent the expected cumulative crater frequency from diameter X to infinity:

n(0.8-5km)=N(0.8 km)-N(5 km)

The cumulative frequencies N(0.8 km) and N(5 km) can be calculated from the canonical Neukum chronology function at N(1 km)

N(1 km)=5.44e-14 [$e^{6.93T}$-1]+8.38e-4T, where T is the model age in billions of years.

Scaling using the Neukum production function:

N(0.8 km)=2.24468*N(1 km)
N(5 km)=0.01384*N(1 km)

So n(0.8-5km)=2.23084*N(1 km).

Text S2. Statistical significance

We tested for the statistical significance of a trend in rock abundance as a function of neighborhood crater frequency with the Mann-Kendall test as implemented by *pyMannKendall* (Hussain and Mahmud, 2019). The table below shows the resulting parameters. There is a statistically significant trend in all of the summary statistics (median, average, 5th-percentile, and 95th-percentile) as well as in a sub-sampled version of the raw data. The trends were strongest as measured by Kendall Tau-B in the average, median, and 95th percentile, consistent with qualitative examination of the data (e.g., Fig. 2a).

	Reject Null Hypothesis	**Trend**	**p**	**Normalized Test Stat**	**Kendall Tau-b (larger negative number; stronger declining trend)**
Median	True	Decreasing	3.55E-15	-7.868	-0.428
Average	True	Decreasing	0.00E+00	-10.164	-0.690
5th	True	Decreasing	3.40E-03	-2.929	-0.059
95th	True	Decreasing	2.22E-09	-5.981	-0.387
Raw Data/ subsampled*	True	Decreasing	0.00E+00	-54.783	-0.124

*For memory reasons, it was impossible to run the full 32million points in the dataset without subsampling. Every 400th point was selected as a subsample. Testing suggests tau_b does not change as a function of sampling, though more points result in a more significant test statistic, as expected.

References:

Hussain, Md. M. and Mahmud, I. (2019). pyMannKendall: a python package for non parametric Mann Kendall family of trend tests. *Journal of Open Source Software*, *4*(39), 1556, https://doi.org/10.21105/joss.01556

Text S3. Additional Monte Carlo Model Description

More details of how the Monte Carlo model works are as follows (*model functions & variables in parentheses)*:

Iterations (*nruns*): Like all Monte Carlo models, this model is iterated a number of times, *nruns*. The multiple trials are important because the sequence of craters is important to the results. We used 1000 runs in all the results reported in this paper.

Space (*domainpx/pxres*): We used a single Diviner pixel as the relevant domain scale (*domainpx* × *domainpx* = 236.9m× 236.9 m). This is divided into cells; we used *pxres* ~2m/px resolution (118 cells × 118 cells).

Time/Age (*endtimeMoon/modeltimestep/neqtime*): For each Monte Carlo iteration, the end of the model run is specified in physical units. We run the model from T=0 to *endtimeMoon* =3.72 Ga in our calculations, and compare the data from 500 Ma to 3.72 Ga to cover the range of the data we gathered. We do not plot the youngest times in Fig. 3 because the model behavior in early times is particularly inaccurate because of the non-inclusion of <5m diameter craters.

The time step in the model was defined as *modeltimestep*=50 Myr; experiments suggest that this does not influence results. The expected number of craters in a given *modeltimestep* in the domain remains constant at every timestep, though the exact number produced at a given size depends on a draw from the Poisson distribution. The model timestep is equivalent to the physical timestep only in the linear part of the NPF (Ivanov, 2001). For the exponential part of the crater chronology, to produce the same number of craters, the equivalent physical timestep is shorter to accommodate the much higher early flux. See the helper function *neqtime* in the code repository in modelparams.py.

Tracked Quantities (*lunarreg, lunarrockfa*): Two quantities are tracked: the regolith thickness (in meters), and rock abundance (meant to be conceptually equivalent to Diviner rock abundance, so a fraction of the area covered by rocks (>=1m), not individual rocks).

Crater, regolith, and rock creation (*drawrocks, drawreg)*: The size range used in the model is from D=5m to 800m craters. The size and number of all the craters produced in a timestep are determined from the NPF (with an extension below 10m using Grun et al. (1985) at 5m-10m), and these craters are added to the domain. Each crater's center position is drawn randomly; the associated regolith added for each crater is calculated using Hirabayashi et al. (2018)'s formulation. Inside the crater cavity, new regolith is only created if it is larger than what exists already; outside, regolith (ejecta) is added to what already exists and declines with distance from the rim as $Dist^{-3}$ (e.g., Melosh, 1989).

Rock areal coverage is added with a heuristic depending first on what fraction *f* of the new crater's interior location had regolith thickness greater than the excavation depth. The new crater rock abundance is $f \times RA_{exc} + RA_{reg}$ in its interior and at its rim, with the excavated rock abundance declining with distance from the rim as $Dist^{-3}$. RA_{exc} is meant to parameterize the rock abundance produced from new bedrock-excavating craters (rocks sourced from bedrock); RA_{exc} specifically is meant to represent the rock abundance of these zero-aged craters proximal

to their rim (i.e., in the model, this is treated as the area with the highest rock abundance and the rock abundance then falls off with distance from the rim, as specified above).   Added only within one crater diameter, RA_{reg} is meant to conceptually reflect the addition of rocks from the regolith volume (at a low rate): it happens whether the excavation depth is exceeded or not (regardless of *f*). Note that, for simplicity, the rock abundance after new craters does not go down. Using the maximum of the new and existing value does neglect the possibility that excavation of regolith could occasionally reduce the rock abundance on surfaces via burial.

Rock destruction (*destroyrocks, halflife*): For every pixel, the areal coverage of rocks is reduced exponentially at a *halflife* specified in the model parameters.

References:

Grün, E., Zook, H.A., Fechtig, H., Giese, R.H. (1985), Collisional balance of the meteoritic complex, *Icarus, 62,* 244-272, doi: 10.1016/0019-1035(85)90121-6.

Hirabayashi, M., Howl, B., Fassett, C., Soderblom, J., Minton, D., & Melosh, H. (2018). The role of breccia lenses in regolith generation from the formation of small, simple craters: Application to the Apollo 15 landing site. *JGR-Planets, 123*, 527– 543.

Ivanov, B. A. (2001), Mars/Moon cratering rate ratio estimates, *Space Sci. Rev*., *96*, 87–104, doi:10.1023/A:1011941121102.

Melosh, H.J. (1989). Impact Cratering: A Geologic Process. Oxford: Oxford Univ. Press, 245pp.

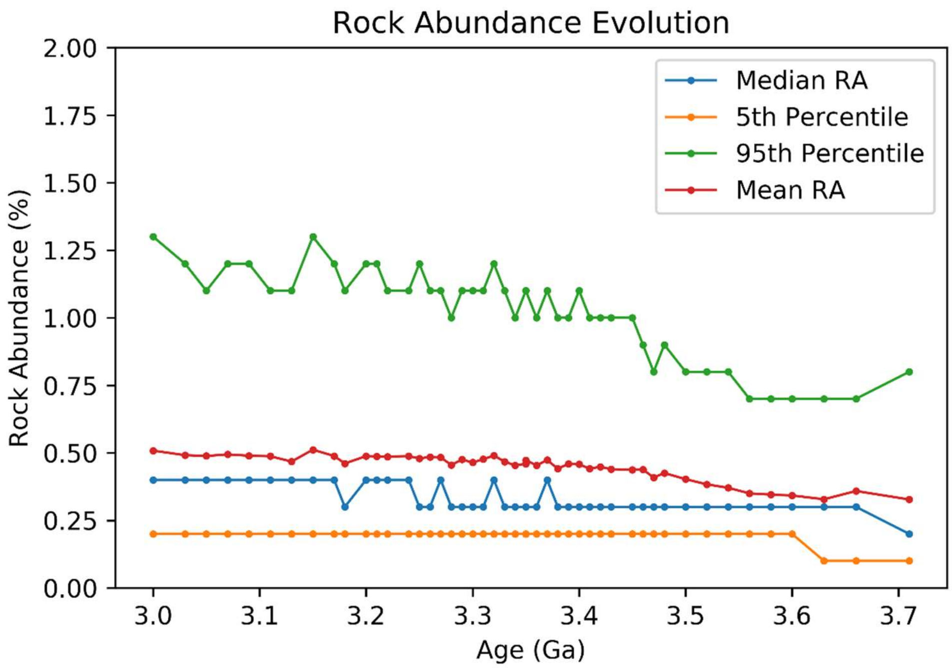

Figure S1. Detail for the rock abundance evolution (from Fig. 2b) for the period before 3 Ga. The trend in how rock abundance varies for surfaces of different age is more pronounced than later in lunar history.

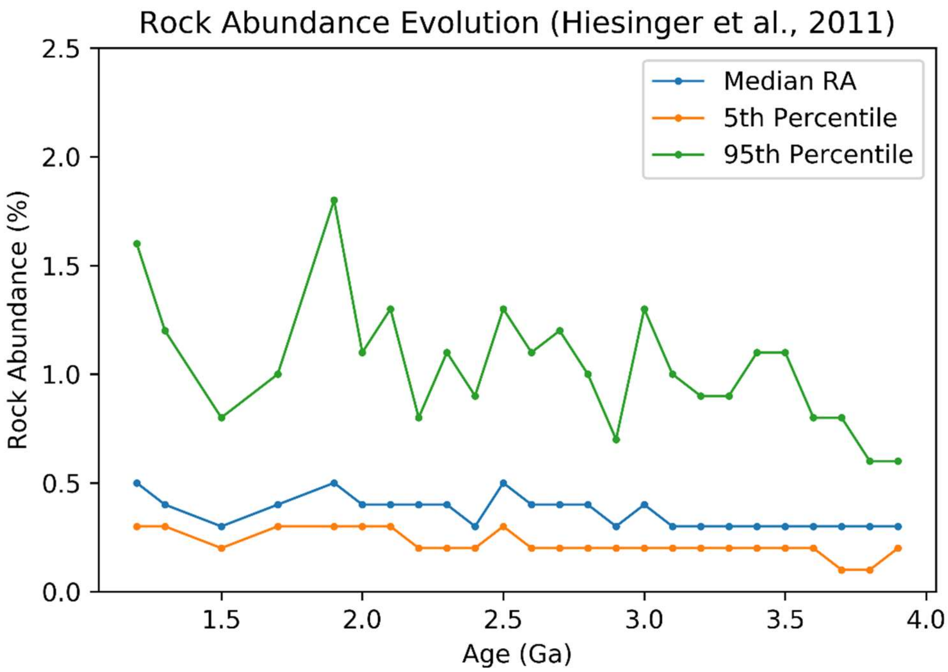

Figure S2. Results for Diviner rock abundance (y-axis) vs Neukum model age in billions of years (x-axis) for units defined in Hiesinger et al., 2010. The Hiesinger unit boundaries used were from a digitization of the original Hiesinger et al. crater counts released by the LROC team. The bin sizes are defined in 100 Ma increments. The statistics are derived in a manner similar to Fig. 2. There is a general decline in the rock abundance, although less pronounced, than using neighborhood crater frequency to determine age.